Journal of Physics and Chemistry of Solids 195 (2024) 112290

Contents lists available at ScienceDirect

Journal of Physics and Chemistry of Solids

journal homepage: www.elsevier.com/locate/jpcs

Correlation between zeta potential and electron paramagnetic resonance of thulium, europium co-doped yttria based suspensions

S.C. Santos *, O. Rodrigues Jr., L.L. Campos

Instituto de Pesquisas Energeticas e Nucleares – IPEN, Av. Prof. Lineu Prestes 2242, Cidade Universitaria, Sao Paulo, Brazil

ARTICLE INFO

Keywords:
Yttria
Europium oxide
Thulium oxide
Rare-earths
Zeta potential
Stability
EPR
Radiation dosimetry
Ceramic processing

ABSTRACT

The formation of advanced ceramic components with homogeneous microstructure and functional characteristics demands a suitable control of particle dispersion. Thus, the characterization of particle stability as immersed in a liquid medium is important. The present paper reports an approach to evaluate the stability of europium, thulium co-doped yttria (YET) nanoparticles by a correlation between zeta potential and Electron Paramagnetic Resonance (EPR) techniques. Based on results, YET suspensions exhibited high stability apart from pH 10, while their isoelectric point presented a slight variation from pH_{IEP} 8.5 to 9.2 according to thulium content 0 and 2 at.%, respectively. The peak-to-peak amplitude of EPR spectra of the YET suspensions increased as pH shifted toward alkaline condition, following zeta potential curves features. The present achievements are very useful parameters to form stable suspensions based on rare-earth oxides and to advance toward new materials for radiation dosimetry.

1. Introduction

Dispersion of particles in an aqueous solvent, with the aim to form a suspension, is one of the most usual procedures in ceramic processing [1]. The structure of a suspension relies on particle characteristics as morphology [2], size distribution [3], density [4], surface area [5], and also the spacial distribution of particles throughout the liquid phase [6].

Zeta potential (ζ) [7] is a key parameter to observe the stability of particles in a liquid solvent, and is calculated [7] by measuring the electrophoretic mobility (με) of particle. In a recent study of the group [8], it was observed that thulium-yttria nanoparticles with mean particle size (d_{50}) of less than 200 nm, exhibited isoelectric point (IEP) between pH_{IEP} 8.5 and pH_{IEP} 9.2, high stability at pH 10.5, with ζ-value of 10.5 mV. In addition, Electron Paramagnetic Resonance (EPR) [9] is a powerful non-destructive and non-invasive characterization technique to observe paramagnetic radicals in materials. Considering that surface features govern the stability behavior of particles immersed in liquid solvent, EPR characterization can be useful to observe how the surface species can induce the dispersion of powders and corroborate zeta potential achievements.

Rare-earth based oxides exhibit a set of special physical and chemical properties [10,11] and whose demand has been increasing substantially for batteries, solar cells [12], fuel cells [13], special alloys [14], catalysis [15], refractories [16], biomarkers [17], and radiation dosimetry [18]. Considering the wide range of applicability of rare-earth based materials, they have been addressed as critical materials by European Union Comission [19] and United States government [20].

Even though rare-earth based oxides are very important materials, studies on powder stability are very scarce. With the aim to contribute with this scientific field, the present work reports a study on the stability of europium, thulium co-doped yttria nanoparticles in aqueous solvent as a function of pH, by an approach of correlating zeta potential and Electron Paramagnetic Resonance techniques. In this purpose the following parameters concerned stability of YET particles in aqueous solvent were evaluated: zeta potential as a function of pH, zeta potential stability during time, isoelectric point (IEP) according to pH and YET particle composition, paramagnetic radicals, g-values of EPR spectra of samples, and peak-to-peak amplitude of the EPR spectra as a function of YET composition and pH. The results achieved in this study are important parameters to advance toward formation of new materials by colloidal processing for radiation dosimetry.

2. Experimental

Europium-thulium co-doped yttria powders (YET) were obtained by using the following starting materials: yttria (Y_2O_3, 99.99 %, Alfa Aesar

* Corresponding author.
E-mail address: silas.cardoso@alumni.usp.br (S.C. Santos).

https://doi.org/10.1016/j.jpcs.2024.112290
Received 10 June 2024; Received in revised form 16 August 2024; Accepted 26 August 2024
Available online 27 August 2024

GmbH), thulium oxide (Tm_2O_3, 99.999 %, Alfa Aesar GmbH), europium oxide (Eu_2O_3, 99.999 %, Alfa Aesar GmbH), nitric acid (HNO_3, Synth), ammonium hydroxide (NH_4OH, Casa Americana), and ethanol (CH_3CH_2OH, Labsynth). The acronym YET comes from the following rare-earth sesquioxides (RE_2O_3), Y as yttria (Y_2O_3), E as europium oxide (Eu_2O_3), and T as thulium oxide (Tm_2O_3).

The synthesis of YET nano-sized powders was based on the hydrothermal method [21], in which the content of the rare-earth dopant was estimated in atomic percentage (at.%) by stoichiometry calculations, and considering yttria as a host reference. The precursor powders were obtained by processing a stock solution at 60 °C for 6 h in a condenser system, followed by a washing cycle using deionized water. The nano-sized ceramic powders were formed by thermal treatment up to 1500 °C for 2 h in air atmosphere using a box furnace (Lindberg Blue, Haake). The YET compositions were formed by varying thulium content from 0.5 at.% up to 2.0 at%, while europium content was fixed at 2.0 at %. The full description and results on YET nano-sized powders are reported in our recent study [22].

The crystalline structure of the YET powders was characterized by X-ray diffraction (XRD, Rigaku Multiflex), at room temperature, angular range (2θ) 25-80°, step size of 0.5°.min^{-1}, and CuK$\alpha_{1,2}$ radiation ($\lambda_{average}$ = 1.54184 Å). The identification of the crystalline structure, as well as the indexing of lattice planes (h, k, l) were performed by Rietveld refinement using Profex [23] software. Additionally, electron density maps were obtained from refinement files of the observed structures. Furthermore, a graphical representation of the crystal lattice was built up by Vesta [24] software.

Particle size distribution (d_{10},d_{50},d_{90}) [25] of the YET powders was determined by Photon Correlation Spectroscopy [26] (PCS, Litesizer500, Anton Paar), in which particle diameter was calculated based on hydrodynamic model [27], according to Eq. (1). Besides, diluted ceramic suspensions were prepared with 0.01 vol% solids at pH 10, which is a suitable condition to provide dispersion of particles by electrostatic mechanism as reported in our previous study [28]. The size and morphology of the YET powders were observed by a Scanning Electron Microscope (SEM, Inca-X, Oxford Instruments).

$$d_h = \left(\frac{K_{BT}}{3\pi\eta(T)D_t}\right)[nm] \quad (1)$$

Where, K_{BT} is the Boltzmann constant (1.38064852.10^{-23} m^2 kg.s^{-2}. K^{-1}), T is the temperature (K), (T) is the viscosity of the suspending liquid and, D_t is the particle diffusion coefficient.

The stability of YET particles dispersed in aqueous solvent was evaluated by electrophoretic mobility (μ_e) measurements, under room temperature (20 °C), followed by zeta potential (ζ) calculation, and using Smoluchowski limit as expressed in Eq. (2) [29]. Stock suspensions containing 0.5 g L^{-1} of YET particles with 1 mM NaCl (58.54 g.Mol−1, Merck) as indifferent electrolyte were prepared. In addition, HCl and KOH solutions were used to shift the pH of stock suspensions from acid to alkaline condition.

$$\zeta = \left(\frac{\mu_e \cdot \eta}{\varepsilon}\right)[mV] \quad (2)$$

Where ε is permittivity of liquid (J.V^{-2} m); η is the viscosity of liquid (cP); μ_e is the electrophoretic mobility of particles (μ.s^{-1}.V^{-1}cm).

The paramagnetic response of YET suspensions were evaluated by electron paramagnetic resonance spectroscopy (EPR), using an X-band magnetic spectrometer (Bruker EMX PLUS). As the EPR technique deals with microwave emission and microwave absorption under a magnetic field, the quality of an EPR spectra basically relies on sample mass and measurement parameters. In this study, three EPR parameters were evaluated as number of scans, from 1 to 10; modulation amplitude (G), from 1 to 4G; and sweep time (s), from 0.24 to 10.02s. In addition, the EPR spectra was recorded using the additional parameters: room atmosphere, field modulation frequency of 100 kHz, microwave power of 2.5 mW, center field of 300 mT, sweep width of 300 mT, time constant of 0.01 ms, temperature of 20°C, controlled humidity, and a DPPH (2, 2-Diphenyl-1-picrylhydrazyl, Bruker) as reference.

All EPR spectra recorded under the present conditions were evaluated taking in account their features as peak-to-peak amplitude (PPA), and g-value (Eq. (3)). Three samples of suspensions were used for each measurement condition, and an average spectra was obtained for evaluation. The normalization of the EPR measurements was performed by dividing the average EPR spectra intensity by sample mass, followed by dividing the result by the peak-to-peak height of the DPPH.

$$g = 714.4775\left(\frac{\nu}{B_0}\right) \quad (3)$$

Where, v is the microwave frequency in hertz (GHz), and B_0 is the magnetic field in gauss (G).

3. Results and discussion

Particle size evolution of YET powders as a function of thulium (Tm) content is illustrated in Fig. 1a. As can be seen, “pure” yttria (0%at. Tm) exhibited the narrowest particle size distribution, where the diameter fractions d_{10}-d_{90} are below 100 nm. On the other hand, dopping yttria with Tm led to formation of powdered compositions with larger particle size distributions probably due to slight changes on crystal lattice and surface features. The most significant Tm effect on particle size was observed for the YET composition with 1.5%Tm, with the following particle size fractions d_{10}, d_{50} and d_{90} as 375, 654, and 913 nm, respectively. Taking in account the pink curve, which corresponds to the 50 % fraction (d_{50}), it is clearly evident that only the composition of 1.5 at.%Tm exhibited the largest particle size, while compositions of 0.0, 1.0, and 2.0 at.Tm% exhibited values of particle size very similar and below 180 nm. It indicates that the processing conditions used to disperse particles was not enough for the specific composition of 1.5 at. %, otherwise, the composition of 2 at.%Tm, which has more Tm content would have presented a larger particle size.

As reported in literature [30–39], surface potential drives the tendency of particles to form agglomerates by creating bonds between particles. In addition particle size has great effect on further stages of

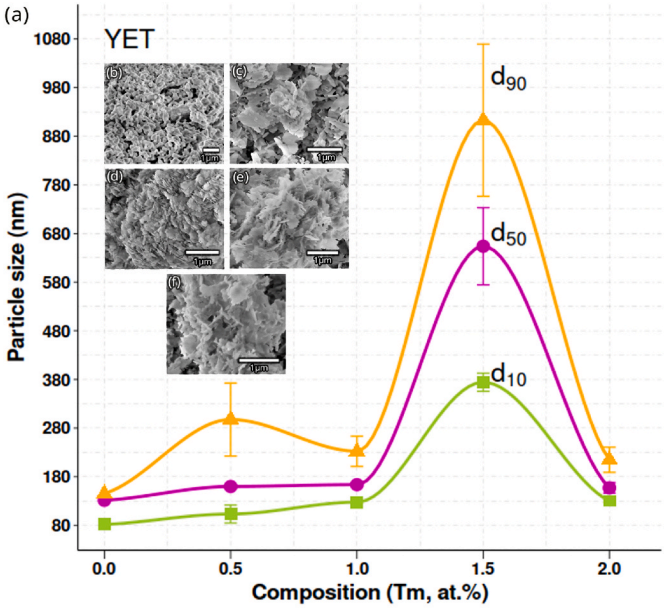

Fig. 1. Powder characterization of the YET compositions as a function of Tm content: (a) particle size distribution with the following diameter size fractions d_{10}, d_{50} and d_{90}; SEM images of the powdered samples (b) YET_0; (c) $YET_{0.5}$; (d) $YET_{1.0}$; (e) $YET_{1.5}$; and (f) $YET_{2.0}$.

processing, including the final features of the material/component produced. Supalak et al. [40] obtained dense alumina based ceramics using a mixture of powders, containing 70 wt% of particles with average size of 3 μm, and 30 wt% of particles with average size of 1.65 μm. Gadow et al. [41] observed that ceramic resins with a larger mean particle size exhibit faster curing and a relatively low sedimentation stability. Liu et al. [42] observed that small/narrow particle distribution of iridium oxide produced by dual-dispersion method appears to be preferred to reduce sedimentation issues and catalyst waste during the ink preparation process, and as a result, reducing production costs. Wu et al. [43] found out that increasing the beeswax (BW) content in lipid phase reduced the solid liquid particle (SLP) size, contributed to the formation of oleofilm with increased crystallinity degree, surface hydrophobicity, light, and water vapor barrier performance.

SEM images of YET powdered compositions prepared with up to 2.0 at.%Tm are illustrated apart from Fig. 1b– f. YET powders without thulium (0 at.%Tm) exhibited agglomerate of rounded particles, whose size is less than 1 μm. On the other hand, it was clearly evidenced that the use of thulium at least 0.5 at%Tm (Fig. 1c) provided remarkable changes on particle shape and size, from round to flackey shape, and size higher than 1 μm. Moreover, increasing Tm content enhanced flacky shape and size of powdered samples, as illustrated from Fig. 1d– f. Considering this achievement, it seems that thulium act as a surfactant agent, by changing particle shape from rounded (no Tm) to flackey (Tm ranging from 0.5 to 2 at.%). Additionally, the size of agglomerates is enhanced according to Tm content, which corroborates with the particle size distribution data from PCS curves (Fig. 1a).

Synthesis methods, which include drying and thermal treatment stages have substantial effect on the relation between growth and crystallization of particles, and as a consequence, drive the size and shape of powdered materials. Sengupta et al. [44] produced triangular/hexagonal particles by using a non-inonic surfactant Triton X-114, while spherical particles were succeeded by using Tween 20. Song et al. [45] found out the permeability of porous media deteriorates as the particle shape deviates from the sphere. Nie et al.[46] reported that the mobility of dry granular flows of large elongated grains is enhanced by increasing the content of finer circular grains. Like size, particle shape is an important parameter in colloidal processing. During a study performed by the group[47], it was found out that ceramic suspensions based on 25 vol% of a rare-earth oxide powdered concentrate (Y, Dy, Eu, Tr, Tm, Lu), with elongated particles, demanded more content of tetramethyl-ammonyum hydroxide (HTMA) to improve the dispersion of particles by electrostatic mechanism.

Zeta potential (ζ) curves of YET suspensions as a function of pH are illustrated in Fig, 2. The range of pH was set from 6 to 14 in consideration that rare-earth particles tend to dissolve in pH-values below 5.5 [48]. "Pure" yttria (light blue line) exhibited an isoelectric point (IEP), the pH-value at which ζ is zero, at pH 9.0 in agreement with literature [49]. A weak condition of stability was observed in a range of pH from 6 to 7.2, where zeta-values were a little bit higher than 20 mV. In addition, from pH 7.2 up to pH 10, all pH-values were inferior than |20|mV, which correspond to an unstable region. Apart from pH 10, conditions of higher stability were obtained, where the maximum stability was achieved at at pH 12 and with a zeta-value of −33mV. These achievements reported here differ a little bit of our study reported in[50], where aqueous suspensions of yttria exhibited a IEP at pH 8.5, and high stability conditions were stablish at pH 5.5, and apart from pH 10. The difference observed between theses studies can be attributed to yttria powders characteristics as size, shape, and chemical composition.

Doping yttria with rare-earth metal(s) led to a substantial change on the surface chemistry of particles, providing a difference response at interface solid-particle-surface/aqueous solvent according to pH. YET suspensions prepared with only europium (YET, 0 at.%Tm) - Fig. 2 presented low stability from pH 6 to 8.7, whereas high stability was achieved at pH-values above 8.8, with a zeta-value near to 30 mV at pH 10. Additionally, it was identified that doping yttria with europium

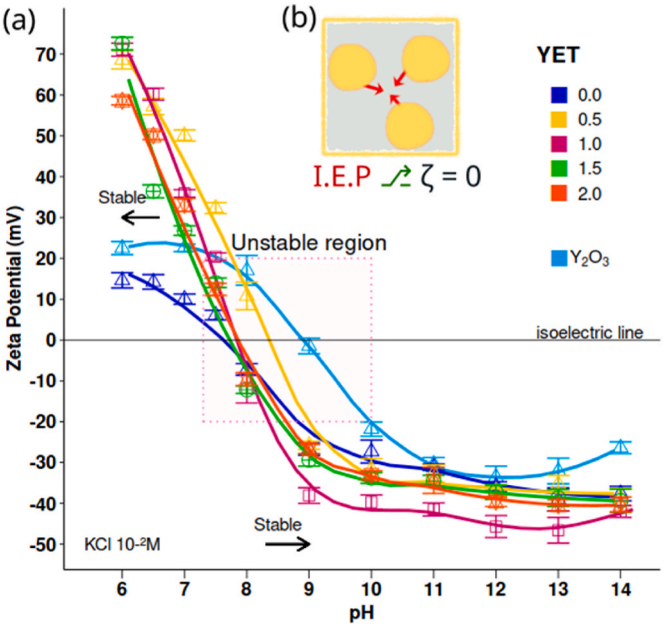

Fig. 2. (a) Zeta potential curves of YET compositions ranging from 0 to 2 at.% Tm as a function of pH, (b) particles come to form agglomerates at IEP, where ζ-value is zero.

provided a remarkable change on IEP of yttria, from pH 9.0 (pure yttria) to 7.6 and as a result, a wider range of stability was observed apart from pH 8.8 until pH 14.

On Fig. 2, the YET 1 at.%Tm suspension exhibited the highest zeta potential values (ζ > 38 mV) among all compositions evaluated. Moreover, it is seen that setting pH-values to 7.5–9 lead YET suspensions to fall into unstable region (light pink square), where attraction forces become more effective, and particles begin to form flocs. In the weak flocculation state, particles form flocs in suspension with at least a minimum equilibrium separation, whereas in strong flocculation state, particles form a particulate network, or clusters [29]. Furthermore, except YET 0 at.%Tm, all YET compositions exhibited also high stability in the range of pH from 6 to 7.4, with ζ-values ranging from 60 to 70 mV. This result is attributed to the balance of charges between Y, Eu and Tm ions that provided a surface potential much more effective for acid condition. Even though YET suspensions exhibited outstanding stability behaviour in lower pH values, previous studies[51–57] revealed that rare-earth particles are usually soluble in acid condition, which means pH values below pH 7. It is also observed that all compositions presented a tendency of decrease ζ-values apart from pH 13, where this effect was more representative for the following compositions Y_2O_3 and YET 1 at.% Tm and YET 2 at.%Tm. As predicted by Stern model[58], a solid particle has a limit of adsorption of ions from suspension during the formation of the electric double layer (EDL). By increasing the ionic strength by pH adjustment to higher values those ions that cannot constitute EDL begin to act as an opposite force to reduce the EDL thickness, thus lower ζ-values are recorded during characterization of samples.

The unstable region highlighted on Fig. 2 illustrates the great effect of co-doping yttria with thulium (Tm) and europium (Eu) on IEP of the powdered compositions. While "pure" yttria exhibited an IEP at pH 8.8, doping it with 2 at%Eu (YET 0 at.%) led to a remarkable shift on its IEP to pH 7.6. Increasing Tm content still provided the displacement of IEP, however in lower magnitude, from pH 7.6 (0%at Tm) to pH 7.8 (2 at.% Tm). The displacement of the IEP of the YET suspensions to lower pH value provide as advantage a wider range of stability of particles which can be achieved apart from pH 8.3. The IEP is a key parameter in colloidal processing. Stable suspensions are usually prepared as pH-value is far prom IEP. At IEP ζ-value is 0 due to no formation of EDL,

and as a consequence, particles are subject of attraction forces as van der Waals, and tend to form agglomerates, as illustrated in Fig. 2b.

It was noticed that both Eu and Tm as activators of yttria also improved its dispersion behaviour in aqueous solvent. This achievement had also been observed in our previous study [8] on thulium-yttria particles, where the use of Tm provided the displacement of IEP of yttria from pH 8.5 to pH 9.2. Additionally, most thulium-yttria based suspensions were highly stabilized at pH 10.5. In ceramic processing, dispersant agents based on large polymer chains are commonly used to provide larger range of pH for stability of particles. Lingling et al.[59] using a polymethacrylate ammonium salt (Dolapix CE 64) induced a great shift on IEP of yttria suspensions from pH 8.7 to 4.0. Moreover, sometimes the IEP of a substance is not observed during zeta evaluation as reported in [60]. In this study, parisite-(Ce) based suspensions in hydroxamate solution did not present an IEP, but only zeta potential values from −40 to 110 mW in the range of pH from 3 to 12, respectively.

A didactic representation of how pH-value is effective on dispersion of $YET_{1.0}$ particles is illustrated from Fig. 3a– h. It is clearly evidenced that $YET_{1.0}$ suspensions prepared at pH-value far from IEP (7.76) exhibited greater dispersion, and during drying formed a uniform ceramic film with small agglomerates, as observed in Fig. 3d– f and g, respectively. While those suspensions prepared at pH-value near IEP, produced ceramic films with non-uniform dispersion of particles and large agglomerates superior than 100 μm, as observed in Fig. 3b and c. A relative dispersion of particles was observed in Fig. 3a– e, and Fig. 3h, with a distribution of large and small agglomerates of particles. These findings corroborate with those observed in zeta potential curves in Fig. 2.

The pH-value is a key parameter in ceramic processing based on colloidal suspensions. As particles are in colloidal scale, they are usually subject of attraction forces as van der Waals. Thus, it is fundamental to promote and enhance the dispersion mechanism to avoid particles to form undesired agglomerates. The promotion of dispersion of particles by adjusting pH of solution/suspension is known as electrostatic dispersion. When a solid particle is immersed in aqueous solvent its surface interacts with ions in solution. Ions with opposite charge of particle (counterions) are attracted and adsorbed on particle surface, forming a dense layer assigned to Stern layer. While those ions with the same charge of particle (coions) are attracted by those ions in Stern layer, they are also repealed by particle, and forming a Diffuse layer. The density of co-ions increases as a function of distance of particle On the other hand, the surface potential (Ψ) decreases according to the distance from the particle surface. The sum of Stern layer and Diffuse layer results in the Electric Double Layer (EDL), which is responsible to drives the dispersion of particles by electrostatic mechanism induced by the pH-value of solution/suspension. Additionally, the surface potential at shear plane, which means those ions that are able to follow the particle during the application of an electrical field, can be calculated and represents the zeta potential of particles. It is commonly reported[61–65] that zeta potential is measured, in fact is a parameter calculated from the measurement of electrophoretic mobility (μ_e) of particles, as expressed in Eq. (2). A complementary and practical discussion on zeta potential was reported by Kosmulski[66].

The stability of ζ-values of the YET suspensions as a function of time is shown in Fig. 4. According to results, despite of YET 2 %, all other compositions exhibited a small variation in ζ-values during 300s of evaluation, which was inferior than 3 mV. This result makes clear that the dispersion mechanism between particles based on electrostatic repulsion is effectively in equilibrium. On the other hand, YET 2 % composition showed a tendency of decrease ζ-values from −45 to −32mV, which indicates the electrochemical equilibrium was not achieved. In addition, ionic strength of the medium induces a compression in EDL thickness by desorption of ions on YET particles surface. The EDL and stability of particles is driven by the sum of adsorption energies (E) in a dispersion system, as follows: solid particles (E_s) + liquid/solvent

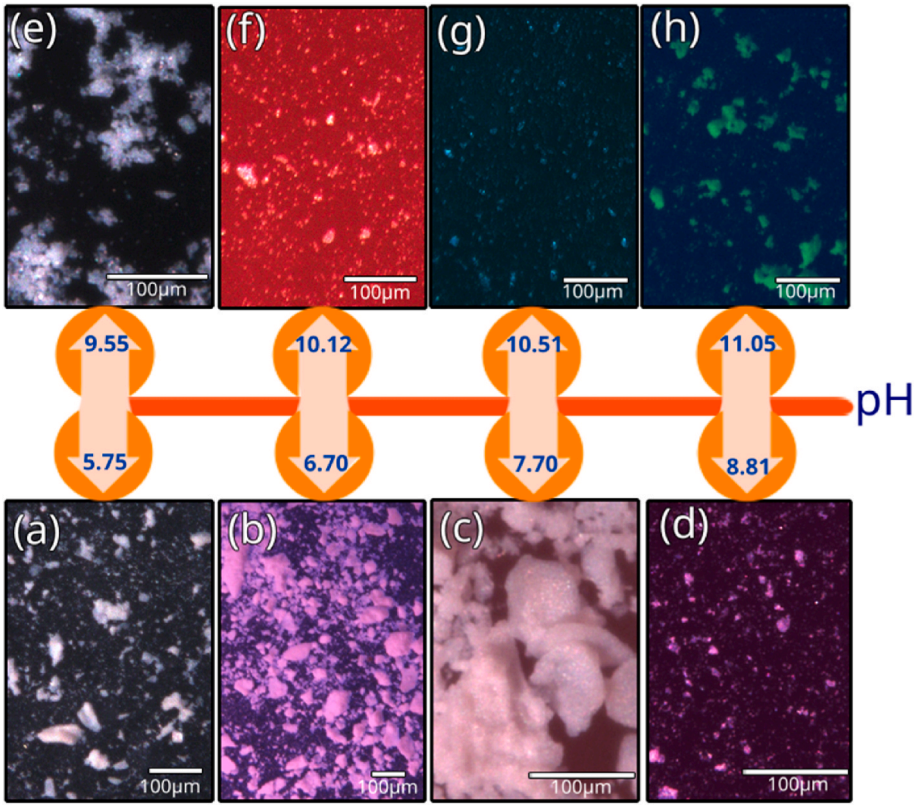

Fig. 3. Effect of pH on dispersion of YET particles in aqueous solvent: OM images of suspensions prepared at pH (a) 5.75, (b) 6.70, (c)7.70, (d) 8.81, (e) 9.55, (f) 10.12, (g) 10.51, (h) 11.05.

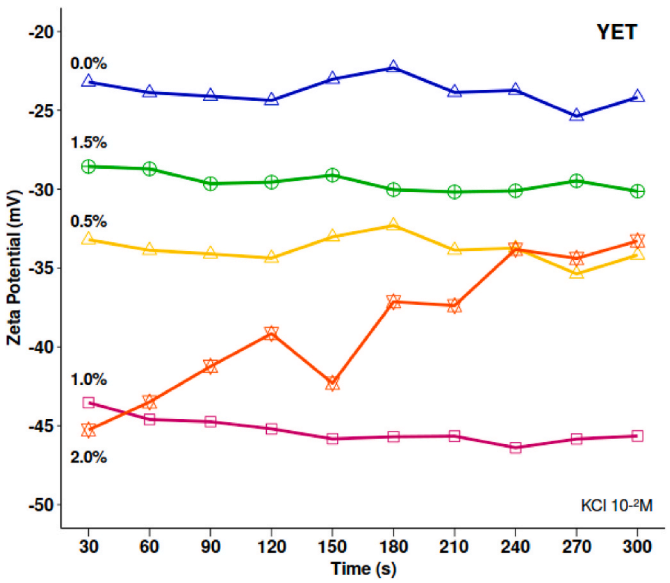

Fig. 4. Evaluation of zeta potential stability of YET suspensions based on different Tm compositions during 300s.

(E_l) - the interface solid/liquid (E_i). Here, the solid interface is YET surface particle, while solvent is water and salts solutions. For YET 2 % suspensions some approaches should be considered to enhance and maintain ζ-values at high levels, as set pH-value to a further alkaline condition and far from IEP, increase homogenization time of suspensions and use less concentrated electrolyte solution (KCl, 10^{-3} M).

The EPR espectra of YET suspensions as a function of pH are illustrated in Fig. 5. According to results, ranging pH from alkaline to acid condition did not induce changes on the shape of EPR spectra (Fig. 5a–c), and no formation of additional resonance peaks either. As reported in our previous study[67], the resonance peak recorded at 160 mT is ascribed to oxygen vacancies provided by both europium ion (Eu^{2+}/Eu^{3+}) and oxygen super oxide ion (O_2^-) from sintering atmosphere. In addition, a significant distinction between EPR spectra have been observed. While YE suspensions exhibited isotropic EPR spectra with sharp shape (Fig. 6a), YET suspensions (Fig. 6b and c) presented EPR spectra with lower intensity and considerable noise, which suggest that using thulium as a second dopant of yttria, in fact, reduced the formation of paramagnetic species by charge compensation, including recombination with those defects previously provided by doping with europium.

Co-doping effect on yttria EPR response, here represented by peak-to-peak amplitude (PPA) of the EPR signal, is clearer illustrated in Fig. 6a–c. For all samples evaluated, higher PPA values were achieved far from IEP, and the most significant were observed at pH 11.0, 10.0, and 12.5 for YE (Fig. 6a), $YET_{0.5}$ (Fig. 6b), and $YET_{1.0}$(Fig. 6c), respectively. The enhancement of the EPR signal follows the behaviour of zeta potential curves (Fig. 2), which means the EPR signal intensity increases as pH moves toward alkaline condition. Besides, as pH value reaches such alkaline condition, the particle surface is fully covered by adsorbed ions (EDL formation). Beyond this condition, those ions that cannot be attached on particle surface (by electrostatic attraction) remains in solution and induces a process of increasing ionic strength of medium. As a result, these free ions compress the EDL of particle by reducing its width and dispersing effect. Moreover, the results indicate that the use of thulium as co-dopant of yttria provided changes on surface chemistry of particles that do not enable satisfactory the adsorption of ions from aqueous solvent, which means the electrochemical reaction was not favourable to form a thick EDL as compared to YE suspensions.

As illustrated in Fig. 7, the pH of suspensions did not induce great influence on g-values of YET samples. For YE suspensions g-values varied from 4.298 at pH 6.8 to 4.295 at pH 10.8. Additionally, for $YET_{0.5}$ suspensions the variation of g-values was quite small, where at extremes of pH scale (pH 5.4 and pH 10.4), both g-values were 4.319. Besides, for $YET_{1.0}$ suspensions g-values varied from 4.324 to 4.315 at pH 5.4 and pH 12.4, respectively.

The use of two rare-earth dopants as europium and thulium had the aim to improve the EPR response of yttria and to form nanoparticles

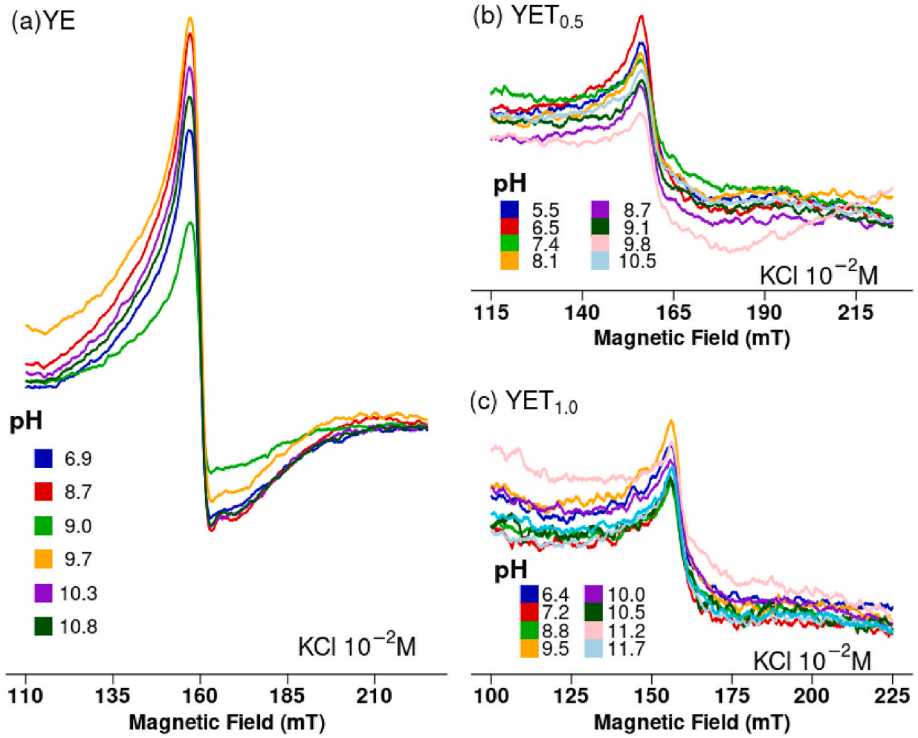

Fig. 5. EPR spectra of YET suspensions as a function of pH recorded in environmental atmosphere and temperature.

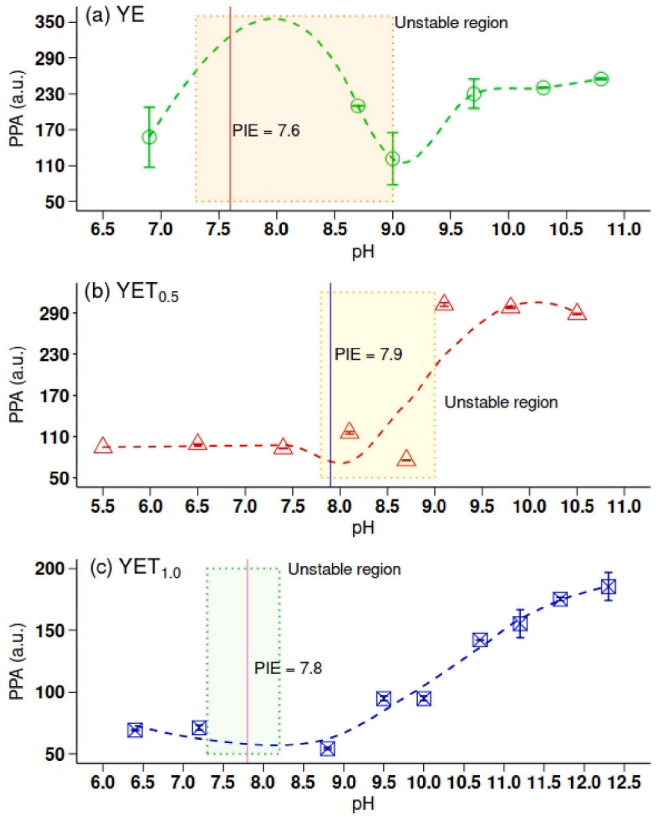

Fig. 6. Peak-to-peak amplitude (PAA) of the YET suspensions as a function of pH: (a) YE, (b)$YET_{0.5}$, and (c) $YET_{1.0}$.

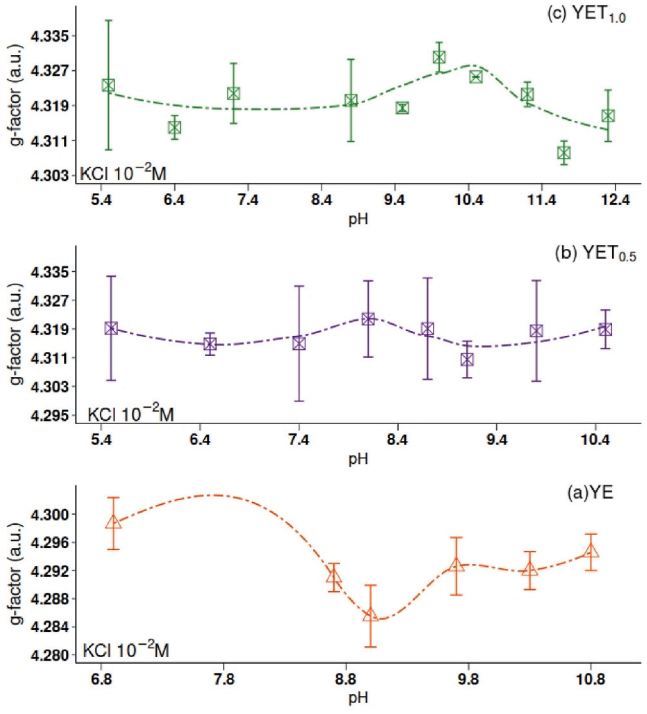

Fig. 7. Variation of g-values of YET suspensions as a function of pH.

with new reactant sites. While the first aim is of great interest of dosimetry application, the second is dedicated to colloidal processing of ceramics. Thus, the control of inter-particle forces is very important to produce ceramic bodies from suspensions with uniform shape and suitable microstructure for an end-use purpose. Based on results, the present work innovates by reporting an approach to correlate zeta potential achievements of YET suspensions with Electron Paramagnetic Resonance characterization. These findings are substantial parameters to advance toward formation of new are-earth based materials for radiation dosimetry.

4. Conclusion

The stability of europium, thulium co-doped yttria nanoparticles (YET) in aqueous solvent as a function of pH was evaluated by a correlation approach between zeta potential and Electron Paramagnetic Resonance (EPR) techniques. Based on zeta potential results, while "pure" yttria and YET_0 suspensions exhibited stability apart from pH 10, all other YET compositions presented high stability in a range of pH from pH 6 to 7, and from pH 10 to 12. The isoelectric point (IEP) of YET particles changed according to thulium content, from pH_{IEP} 8.5 to 9.2. According to EPR results, the peak-to-peak amplitude (PPA) of the EPR spectra of the YET suspensions increased following zeta potential features, where higher values of PPA were achieved in alkaline condition. Moreover, g-value of the YET samples presented a narrow variation as a function of pH. These findings are substantial parameters to advance toward formation of new rare-earth based materials for radiation dosimetry.

5. Current future and developments

Particle stability in aqueous solvent is an important topic in materials science, seeing that its applicability takes place since agriculture up to nuclear technology. Even though zeta potential is a mature technique to evaluate particle stability, the complement of an additional technique is very useful to corroborate the findings, and also to understand other phenomena that could not be observed using only one technique. Moreover, it is fundamental do advance toward studies on how ionizing radiation changes particle surface and its behavior as dispersed in aqueous solvent. Besides, the microstructure formation based on irradiated particles is worth of investigation.

Funding

The authors would like to acknowledge the following sponsor organizations: São Paulo Research Foundation (FAPESP, grant# 2018/05982-0; grant#2022/06695-0), National Council for Scientific and Technological Development (CNPq, grant# 426513/2018-5), and Coordination for the Improvement of High Degree People (CAPES, grant#88882.315568/2019–01).

Availability of data and materials

The raw/processed data required to reproduce these findings cannot be shared at this time due to technical or time limitations.

Ethics and consent to participate

No human or animal were used in the study.

Consent for publication

We authors declare our consent for publication.

CRediT authorship contribution statement

S.C. Santos: Writing – review & editing, Writing – original draft, Methodology, Investigation, Formal analysis, Conceptualization. **O. Rodrigues:** Validation, Software, Resources, Data curation. **L.L. Campos:** Visualization, Supervision, Resources, Funding acquisition.

Declaration of competing interest

The authors declare that they have no known competing financial interests or personal relationships that could have appeared to influence the work reported in this paper.

Data availability

The authors do not have permission to share data.

Acknowledgments

We authors are deeply grateful to Dr. Maria Elisa Chuery Martins Rostelato from Radiation Technology Centre (CTR), Dr. Ivana Conte Cosentino from Science and Technology of Materials Centre (CCTM) both at Nuclear and Energy Research Institute (IPEN/CNEN-SP, Sao Paulo, Brazil). In addition to the following sponsor organizations: São Paulo Research Foundation (FAPESP), grant#2022/06695-0; National Council for Scientific and Technological Development (CNPq); and Coordination for Improvement of High Degree People (CAPES).

This research used facilities of the Brazilian Nanotechnology National Laboratory (LNNano), part of the Brazilian Centre for Research in Energy and Materials (CNPEM), a private non-profit organization under the supervision of the Brazilian Ministry for Science, Technology, and Innovations (MCTI). The (Electron Microscopy) staff is acknowledged for the assistance during the experiments (SEM-FIB-C1-20222260).

References

[1] S.C. Santos, O. Rodrigues, L.L. Campos, Bio-prototyping of europium-yttria based rods for radiation dosimetry, Mater. Chem. Phys. (2017), https://doi.org/10.1016/j.matchemphys.2017.07.063.

[2] N. Doebelin, R. Kleeberg, Profex: a graphical user interface for the Rietveld refinement program, J. Appl. Crystallogr. 48 (2015) 1573–1580, https://doi.org/10.1107/S1600576715014685.

[3] K. Momma, F. Izumi, VESTA: a three-dimensional visualization of crystal, volumetric and morphology data, J. Appl. Crystallogr. 44 (2011) 1272–1276, https://doi.org/10.1107/S0021889811038970.

[4] M. Wedd, S. Ward-Smith, A. Rawle, in: P. Worsfold, C. Poole, A. Townshend, M.B. T.-E. of A.S, Third E. Miró (Eds.), Particle Size Analysis☆, Academic Press, Oxford, 2019, pp. 144–157, https://doi.org/10.1016/B978-0-12-409547-2.14522-6.

[5] W. Tscharnuter, Photon Correlation Spectroscopy in Particle Sizing, John Wiley & Sons Ltd, United States of America, 2000. http://www.brookhaveninstruments.com/literature/lit_90Plus.html.

[6] L. Vamos, P. Jani, Particle sizing by photon correlation laser Doppler anemometer in the submicron/nanometer size range, Opt. Eng. 49 (2010), https://doi.org/10.1117/1.3292002.

[7] D.N. Thomas, S.J. Judd, N. Fawcett, Flocculation modelling: a review, Water Res. 33 (1999) 1579–1592, https://doi.org/10.1016/S0043-1354(98)00392-3.

[8] Y. Zhao, J. He, B. Li, Z. Gao, Q. Guo, Z. Ma, Y. Liu, The role of ceramic particles on the crack inhibition and mechanical properties improvement of Haynes 230 alloy fabricated by laser powder bed fusion, J. Mater. Process. Technol. 320 (2023) 118124, https://doi.org/10.1016/j.jmatprotec.2023.118124.

[9] K. Sekiguchi, K. Katsumata, H. Segawa, T. Nakanishi, A. Yasumori, Effects of particle size, concentration and pore size on the loading density of silica nanoparticle monolayer arrays on anodic aluminum oxide substrates prepared by the spin-coating method, Mater. Chem. Phys. 277 (2022) 125465, https://doi.org/10.1016/j.matchemphys.2021.125465.

[10] R. Qi, Z. Li, H. Zhang, H. Fu, H. Zhang, D. Gao, H. Chen, CO2 capture performance of ceramic membrane with superhydrophobic modification based on deposited SiO2 particles, Energy 283 (2023) 129202, https://doi.org/10.1016/j.energy.2023.129202.

[11] C. Peppersack, A. Kwade, S. Breitung-Faes, Selective particle size analysis in binary submicron particle mixtures using density dependent differential sedimentation, Adv. Powder Technol. 32 (2021) 4049–4057, https://doi.org/10.1016/j.apt.2021.09.010.

[12] H. Kalman, Bulk densities and flowability of non-spherical particles with mono-sized and particle size distributions, Powder Technol. 401 (2022) 117305, https://doi.org/10.1016/j.powtec.2022.117305.

[13] S. Jeon, X. Liu, C. Azersky, J. Ren, S. Zhang, W. Chen, R.W. Hyers, K. Costa, M. Kolbe, D.M. Matson, Particle size effects on dislocation density, microstructure, and phase transformation for high-entropy alloy powders, Materialia 18 (2021) 101161, https://doi.org/10.1016/j.mtla.2021.101161.

[14] J. Huang, H. Chen, J. Yang, T. Zhou, H. Zhang, Effects of particle size on microstructure and mechanical strength of a fly ash based ceramic membrane, Ceram. Int. 49 (2023) 15655–15664, https://doi.org/10.1016/j.ceramint.2023.01.157.

[15] G.C. Girondi Delaqua, F. Vernilli, S.R. Teixeira, H.A. Lopera Colorado, S. N. Monteiro, C.M. Fontes Vieira, Influence of glass particle size on the physico-mechanical properties of red ceramic, J. Mater. Res. Technol. 26 (2023) 6942–6954, https://doi.org/10.1016/j.jmrt.2023.09.040.

[16] Y. Du, D. Ma, B. Pan, N. Sun, Y. Wei, M. Sun, C. Wu, Z. Wang, Q. Li, G. Shi, Preparation and characterization of all-particle SiC ceramic filters, Ceram. Int. (2023), https://doi.org/10.1016/j.ceramint.2023.10.128.

[17] L. Chen, H. Ma, Z. Sun, Y. Zhang, Flowability of multi-sized mixed particles based on shotcrete aggregates, Powder Technol. 408 (2022) 117760, https://doi.org/10.1016/j.powtec.2022.117760.

[18] S. Manotham, P. Tesavibul, Effect of particle size on mechanical properties of alumina ceramic processed by photosensitive binder jetting with powder spattering technique, J. Eur. Ceram. Soc. 42 (2022) 1608–1617, https://doi.org/10.1016/j.jeurceramsoc.2021.11.062.

[19] W. Yared, R. Gadow, The influence of particle size distribution on the curing behavior of ceramic-filled resins for vat photopolymerization, Ceram. Int. 49 (2023) 24156–24164, https://doi.org/10.1016/j.ceramint.2022.11.193.

[20] C. Liu, M. Luo, R. Zeis, P.-Y. Abel Chuang, R. Zhang, S. Du, P.-C. Sui, Fabrication of catalyst layer for proton exchange membrane water electrolyzer: I. Effects of dispersion on particle size distribution and rheological behavior, Int. J. Hydrogen Energy 52 (2024) 1143–1154, https://doi.org/10.1016/j.ijhydene.2023.08.154.

[21] Y. Wu, Y. Li, B. Li, Y. Wu, S. Liu, Improvement of oleofilm performance by regulating the composition and size of emulsion-based solid lipid particle dispersion, Food Hydrocolloids 151 (2024) 109784, https://doi.org/10.1016/j.foodhyd.2024.109784.

[22] I. Sengupta, S. Pareek, P. Bhargava, Surfactant mediated silver synthesis: influence of surfactant molecular structure on the size and shape of silver particles, Inorg. Chem. Commun. 159 (2024) 111675, https://doi.org/10.1016/j.inoche.2023.111675.

[23] H. Song, J. Xie, P. Yin, H. Fu, Y. Zhang, C. Yan, The investigation of the particle shape effect on the permeability of porous media through lattice Boltzmann simulation and experimental study, Int. J. Therm. Sci. 201 (2024) 108983, https://doi.org/10.1016/j.ijthermalsci.2024.108983.

[24] J.-Y. Nie, Y. Cui, Z. Wu, L. Zhang, J. Fang, DEM study on role of fines in mobility of dry granular flows considering particle size-shape correlation, Comput. Geotech. 166 (2024) 105980, https://doi.org/10.1016/j.compgeo.2023.105980.

[25] S.C. Santos, C. Yamagata, S. Mello Castanho, Lighting by biogas burners: perspectives on development in Brazil, J. Mater. Sci. Appl. 5 (2014) 660–673.

[26] R. Sprycha, J. Jablonski, E. Matijević, Zeta potential and surface charge of monodispersed colloidal yttrium(III) oxide and basic carbonate, J. Colloid Interface Sci. 149 (1992) 561–568, https://doi.org/10.1016/0021-9797(92)90443-P.

[27] R. Moreno, Reología de suspensiones cerámicas, Consejo Superior de Investigaciones Científicas, Spain, 2005.

[28] S.C. Santos, L.F.G. Setz, C. Yamagata, S.R.H. Mello-Castanho, Rheological study of yttrium oxide aqueous suspensions. https://doi.org/10.4028/www.scientific.net/MSF.660-661.712, 2010.

[29] M. Kosmulski, Attempt to determine pristine points of zero charge of Nb2O5, Ta2O5, and HfO2, Langmuir 13 (1997) 6315–6320, https://doi.org/10.1021/la970469g.

[30] Y.A. Nechayev Sheyin, V. N, Ions specific absorption on oxides, Kolloid. Zh 41 (1979).

[31] B. Vaziri Hassas, M. Rezaee, S.V. Pisupati, Precipitation of rare earth elements from acid mine drainage by CO2 mineralization process, Chem. Eng. J. 399 (2020) 125716, https://doi.org/10.1016/j.cej.2020.125716.

[32] Z. Hammache, S. Bensaadi, Y. Berbar, N. Audebrand, A. Szymczyk, M. Amara, Recovery of rare earth elements from electronic waste by diffusion dialysis, Separ. Purif. Technol. 254 (2021) 117641, https://doi.org/10.1016/j.seppur.2020.117641.

[33] P. Kim, A. Anderko, A. Navrotsky, R.E. Riman, Trends in structure and thermodynamic properties of normal rare earth carbonates and rare earth hydroxycarbonates, Minerals 8 (2018), https://doi.org/10.3390/min8030106.

[34] A.M. Kaczmarek, K. Van Hecke, R. Van Deun, Nano- and micro-sized rare-earth carbonates and their use as precursors and sacrificial templates for the synthesis of new innovative materials, Chem. Soc. Rev. 44 (2015) 2032–2059, https://doi.org/10.1039/C4CS00433G.

[35] T. Andelman, S. Gordonov, G. Busto, P.V. Moghe, R.E. Riman, Synthesis and cytotoxicity of Y2O3 nanoparticles of various morphologies, Nanoscale Res. Lett. 5 (2009) 263, https://doi.org/10.1007/s11671-009-9445-0.

[36] S.C. Santos, O. Rodrigues, L.L. Campos, Dispersion of thulium-yttria nanoparticles to build up smart structures, Mater. Today Commun. 26 (2021) 101749, https://doi.org/10.1016/j.mtcomm.2020.101749.

[37] L. Jin, X. Mao, S. Wang, M. Dong, Optimization of the rheological properties of yttria suspensions, Ceram. Int. 35 (2009) 925–927, https://doi.org/10.1016/j.ceramint.2008.03.009.

[38] C.L. Owens, G.R. Nash, K. Hadler, R.S. Fitzpatrick, C.G. Anderson, F. Wall, Zeta potentials of the rare earth element fluorcarbonate minerals focusing on bastnäsite and parisite, Adv. Colloid Interface Sci. 256 (2018) 152–162, https://doi.org/10.1016/j.cis.2018.04.009.

[39] H. Guo, X. Gao, K. Yu, X. Wang, S. Liu, Ion adsorption on nanofiltration membrane surface and its effect on rejection of charged solutes: a zeta potential approach, Separ. Purif. Technol. 326 (2023) 124830, https://doi.org/10.1016/j.seppur.2023.124830.

[40] A. Fürst, I. Shahzadi, Z.B. Akkuş-Dağdeviren, A.M. Schöpf, R. Gust, A. Bernkop-Schnürch, Zeta potential shifting nanoemulsions comprising single and gemini tyrosine-based surfactants, Eur. J. Pharmaceut. Sci. 189 (2023) 106538, https://doi.org/10.1016/j.ejps.2023.106538.

[41] V.D. Sobolev, A.N. Filippov, V.M. Starov, Influence of flow and charge transfer inside membranes on measurements of membrane zeta potential, J. Mol. Liq. 323 (2021) 114865, https://doi.org/10.1016/j.molliq.2020.114865.

[42] C. Cherpin, D. Lister, F. Dacquait, S. Weerakul, L. Liu, Magnetite (Fe3O4) and nickel ferrite (NiFe2O4) zeta potential measurements at high temperature: Part II – results, study of the influence of temperature, boron concentration and lithium concentration on the zeta potential, Colloids Surf. A Physicochem. Eng. Asp. 647 (2022) 129030, https://doi.org/10.1016/j.colsurfa.2022.129030.

[43] M. Walters, S. Al Aani, P.P. Esteban, P.M. Williams, D.L. Oatley-Radcliffe, Laser Doppler electrophoresis and electro-osmotic flow mapping for the zeta potential measurement of positively charged membrane surfaces, Chem. Eng. Res. Des. 159 (2020) 468–476, https://doi.org/10.1016/j.cherd.2020.04.022.

[44] M. Kosmulski, Misconceptions in the measurements of zeta potentials in ethylene glycol-based heat transfer fluids, Appl. Therm. Eng. 209 (2022) 118282, https://doi.org/10.1016/j.applthermaleng.2022.118282.